Flow, Turbulence and Combustion (2026) 117:22
https://doi.org/10.1007/s10494-026-00745-z

RESEARCH

A Combustion Model Validation Framework for Turbulent Premixed Hydrogen-Air Flames Utilizing *OpenFOAM*

Svenja Nerzak[1] · Ludovico Nista[1] · Marco Vivenzo[1] · Michael Gauding[1] · Heinz Pitsch[1]

Received: 22 February 2026 / Revised: 21 March 2026 / Accepted: 25 March 2026
© The Author(s) 2026

Abstract
Developing accurate and robust combustion models is challenging, and their validation can be equally demanding. Even when suitable experimental or numerical datasets are available, setting up and performing validation simulations often requires substantial resources. As a result, most validation studies focus on a single dataset from experiments or numerical simulations, which is generally insufficient for a comprehensive model assessment. Systematic model evaluation, therefore, benefits from a comprehensive, standardized, and easy-to-use validation framework containing multiple validation datasets. This paper introduces a validation framework for combustion models and demonstrates its application to a state-of-the-art flamelet model for large-eddy simulations. The framework deploys the open-source *OpenFOAM* toolbox to provide an openly accessible simulation standard allowing straightforward integration of newly developed models and facilitating the adoption by the research community. It includes eight validation cases based on both experimental data and direct numerical simulations, and is designed to be readily expandable by the community to accommodate an arbitrarily large number of additional cases. For all cases, the reference data, together with the required configurations and mesh files, are provided. The framework facilitates the systematic assessment of combustion models by automatically performing simulations for all cases and providing comparisons between model predictions and reference data. As a demonstration, a flamelet-based model for lean premixed hydrogen combustion is implemented in *OpenFOAM* and evaluated within the proposed framework, providing insights into the model's capabilities and limitations across different flow and combustion conditions.

Keywords LES model · Validation framework · *OpenFOAM* · Hydrogen · Thermodiffusive instabilities

✉ Svenja Nerzak
s.nerzak@itv.rwth-aachen.de

[1] Institute for Combustion Technology, RWTH Aachen University, Templergraben 64, 52062 Aachen, Germany

Published online: 23 July 2026

1 Introduction

The design and optimization of next-generation combustion systems rely heavily on predictive numerical simulations, where large-eddy simulation (LES) is a relatively accurate and cost-efficient modeling approach. In this regard, LES combustion models must be continually improved and systematically evaluated to ensure accurate predictions across a broad range of operating conditions, flow regimes, and geometrical configurations (Pope 2000; Pitsch 2006; Barlow 2024). In practice, however, model performance is often assessed on the basis of only a limited set of canonical flame configurations or operating conditions. This limitation arises from the significant effort and complexity associated with comprehensive validation studies in terms of case setup, mesh generation, specification of boundary conditions, and achieving satisfactory agreement with reference cases, such as cold-flow data or conditions, where the model that is to be tested is not relevant (Pitsch 2024). Such single-case or narrowly focused validations are often insufficient to assess model robustness and generalizability across different conditions and geometries. Consequently, the systematic validation and comparison of LES combustion models remain both incomplete and not sufficiently standardized. This, in turn, slows the development of improved modeling formulations and limits their reliability for predictive, model-based design and optimization of next-generation combustion systems.

To address these challenges, a community-accessible validation framework is introduced and designed to enable the systematic, reproducible, and quantitative assessment of LES combustion model formulations across multiple configurations and regimes. The baseline concept of the framework builds upon successful approaches from other research fields, such as the astrophysics community (Calder and Townsley 2019; Calder et al. 2002; Mao et al. 2018) or the turbulence community with the John Hopkins turbulence databases (Kanov et al. 2015), and complements established combustion validation efforts, such as the Turbulent Non-Premixed Flame Workshop (TNF) (Barlow 2024), Sandia turbulent methane-air flame test cases (Barlow and Frank 1998; Barlow et al. 2005), the BLASTNet Simulation Dataset (Chung et al. 2024), which includes a large number of reacting and non-reacting high-fidelity simulation datasets, and the HYLON burner (Marragou et al. 2023; Aniello et al. 2022, 2023) for hydrogen combustion in a dual-swirl coaxial injector configuration. In contrast to TNF-type efforts, where many models and codes are applied in simulations of the same validation case, mostly to support physical understanding (Dillon et al. 2026), the concept here is to apply one model to many data sets, mainly to support validation. The validation framework is designed to be modular and extensible, allowing researchers to integrate additional test cases and LES combustion models easily, thereby ensuring continued relevance as improved model formulations and additional validation datasets become available. Consistent with this open and flexible philosophy, the framework is implemented using the open-source computational fluid dynamics (CFD) software *OpenFOAM*, chosen for its wide accessibility and strong adoption within the CFD community. The framework comprises standardized configurations, including validation data, analysis tools for systematic comparison across multiple configurations, and a driver that automatically executes all included cases and compares results with numerical and experimental reference data.

Given the ongoing transition towards a carbon-neutral energy sector, in which hydrogen is positioned as a promising alternative to fossil fuels (United Nations 2015; Eu 2019; Pitsch 2024), the present implementation focuses on hydrogen combustion modeling. Hydrogen

combustion poses significant technical challenges, including combustion instabilities, flashback, and potentially increased nitrogen oxide (NO_x) emissions (Im and Chen 2002; Berger et al. 2022c; Pitsch 2024), making it an ideal testbed for the evaluation of LES combustion models.

In this context, lean premixed flames are of particular relevance for hydrogen combustion, as their reduced flame temperature leads to lower NO_x emissions compared to stoichiometric conditions. Several studies demonstrated that lean premixed hydrogen-air flames are highly susceptible to thermodiffusive instabilities (TDI), which enhance flame surface area and local reactivity, thereby significantly increasing flame propagation speed (Day et al. 2009; Berger et al. 2022a, b, 2023; Lapenna et al. 2023; Howarth et al. 2023, 2024; Li et al. 2025; Bae et al. 2025). Furthermore, elevated pressure levels, as encountered in internal combustion engines or gas turbines, were found to amplify TDI and the ratio of turbulent to laminar flame speed. This effect results from the increased sensitivity of flame speed and thickness to equivalence ratio variations, with high-pressure flames responding more strongly to fast molecular diffusion of hydrogen into the reaction front (Rieth et al. 2023).

Capturing these effects in LES remains challenging, as the molecular transport driving TDI is typically not fully resolved on the computational grid. Moreover, although TDI originate at the smallest scales, they can strongly influence large-scale quantities and overall flame dynamics (Pitsch 2024), and are further intensified at high Reynolds numbers due to their synergistic interaction with turbulence (Berger et al. 2022c; Aspden et al. 2024; Howarth et al. 2023; Hunt and Aspden 2025; Lapenna et al. 2023). As a result, LES models that explicitly account for TDI remain scarce. Existing approaches include a thickened flame model proposed by Aniello et al. (2022) or Schuh et al. (2024), a flame surface density model by Lapenna et al. (2025), a fractal modeling approach by Ramirez et al. (2025), a filtered tabulated chemistry approach by Dillon et al. (2026), a flamelet generated manifold approach by Pérez-Sánchez et al. (2025), and a tabulated chemistry approach by Berger et al. (2025). This highlights the need of a validation framework to first assess existing models under various operating conditions, and second, to develop improved modeling strategies.

The current implementation comprises eight representative validation cases, some of which were selected at the 16^{th} TNF workshop (Barlow 2024). These include three direct numerical simulation (DNS) of a laminar, two-dimensional statistically planar flame with different equivalence ratios, three DNS datasets of a slot burner spanning a range of Karlovitz numbers (Berger et al. 2024), and two experimental configurations, namely the TU Darmstadt piloted turbulent jet burner (Shi et al. 2024) and the NTNU bluff-body burner (Æsøy and Dawson 2024). Together, these cases cover different levels of flow and flame complexity and capture distinct physical mechanisms, particularly variations in Reynolds and Karlovitz numbers, shear-layer dynamics, and the influence of recirculation zones. The included validation cases represent a starting point and should ultimately be expanded to include several tens of cases, for instance by incorporating datasets from BLASTNet (Chung et al. 2024). Additionally, to demonstrate the capabilities of the validation framework, an open-source implementation of a state-of-the-art combustion model for hydrogen-air flames, derived from Berger et al. (2025), is also provided, along with the chemical reaction mechanisms used to generate the corresponding flamelet libraries. The results of this model can, if desired, be used as a reference for comparison with other models. The framework allows existing and newly developed combustion models to be easily integrated, tested, and evaluated in a consistent and reproducible manner. The overarching goal is to

establish an open validation infrastructure that can serve as a reference for the combustion community.

The paper is organized as follows. Details of the validation framework and the flame configurations are given in Sect. 2. The LES combustion model used as an example is described in Sect. 3. The output of the validation framework is discussed in Sect. 4. Strategies for reusability and standardization of the validation framework are presented in Sect. 5.

2 Validation Framework Based on *OpenFOAM*

The structure and technical implementation of the proposed validation framework are described in the following. The framework is designed to automatically run LES for all the included test cases using the open-source CFD toolbox, *OpenFOAM* (Weller et al. 2023). A schematic overview of the framework's architecture and workflow is shown in Fig. 1.

The framework comprises three main components: (i) the definition and setup of validation test cases, (ii) an automatic runner for CFD simulations, and (iii) a postprocessing module for visualization and quantitative data analysis using the corresponding validation datasets. The framework is designed to be easily coupled with user-defined combustion models (via the "Model Development" module) through flexible and customizable *OpenFOAM*-based routines, thereby also facilitating the sharing of model formulations within the community. To demonstrate its workflow, a state-of-the-art combustion model, tailored for modeling lean premixed hydrogen flames, is provided as part of the distribution (Sect. 3). Nevertheless, the validation framework itself is model-agnostic and is not restricted to this specific implementation.

2.1 Validation Data

The validation framework currently includes a set of reference cases derived from four hydrogen-air flame configurations: a laminar two-dimensional thermodiffusively-unstable statistically planar flame and three-dimensional turbulent slot, jet, and bluff-body flames.

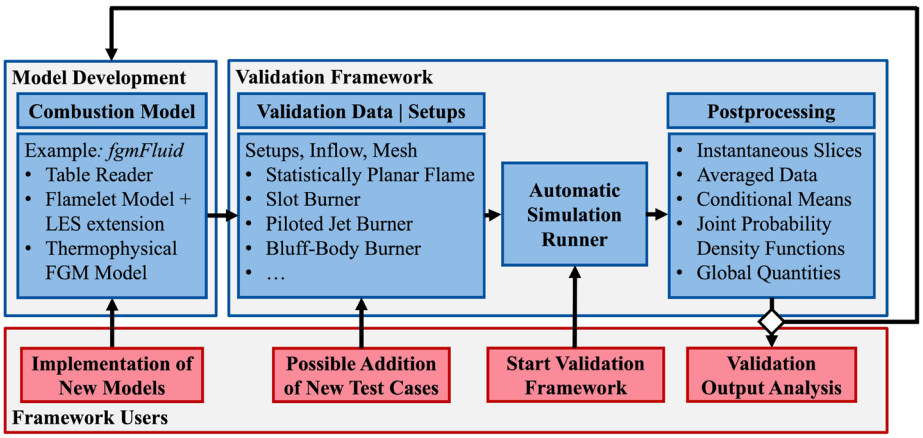


Fig. 1 Schematic representation of the proposed validation framework workflow utilizing the *OpenFOAM* CFD solver

For the statistically planar flame and for the slot flame, three different operating conditions are provided each, resulting in a total of eight validation cases. Experimental validation data are provided for the jet and bluff-body flames, while for the statistically planar flame and the slot flame, DNS data are included within the framework. The framework follows a hierarchical validation strategy, progressing from canonical configurations to more complex turbulent flames following the validation pyramid shown in Fig. 2 (Pitsch and Trisjono 2014; Pitsch 2024).

Together, these cases cover increasing levels of geometric and physical complexity and exhibit key flow and combustion phenomena, such as shear layers, curvature effects, and recirculation zones. Such features can strongly interact with TDI, making them essential for assessing a model's capability to accurately represent turbulence-chemistry interaction (TCI). At the same time, the selected cases enable users to demonstrate model performance across a broad range of operating conditions and combustion regimes. Currently, the turbulent validation cases focus on an equivalence ratio of $\phi = 0.4$, whereas three ϕ values are considered for the laminar cases. This choice is motivated by the fact that $\phi = 0.4$ cases exhibit strong TDI (Berger et al. 2022b), making them particularly suitable for analyzing TCI. Further cases with varying ϕ will be added in the future. Finally, the use of *OpenFOAM* also facilitates the inclusion of test cases at the system level.

Detailed descriptions of the validation data and all relevant parameters are provided in the following sections, while the corresponding *OpenFOAM* simulation setups are described in Sect. 2.2. Owing to the modular structure of the framework, additional validation cases can be incorporated following the setup of the existing cases. The validation data are provided on the research data management platform Coscine (RWTH Aachen University 2016), together with the corresponding metadata, in accordance with the research data management guidelines of the German Research Foundation (DFG) and the FAIR principles established by Wilkinson et al. (2016). A script, *validationData.py*, is included in the framework to interact with the Coscine API to automatically download the data.

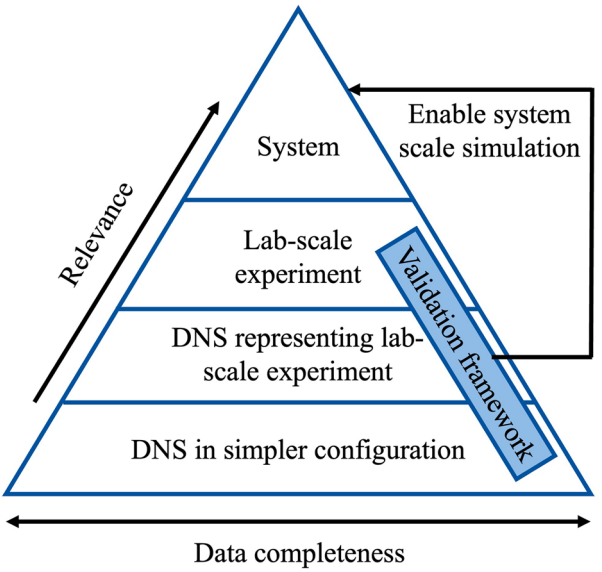


Fig. 2 Validation pyramid illustrating the hierarchical approach on which the present validation framework is based (Pitsch and Trisjono 2014; Pitsch 2024)

2.1.1 Laminar Two-Dimensional Statistically Planar Flame

The setup of the laminar two-dimensional statistically planar flame is shown in Fig. 3. The configuration is selected for the framework as a baseline to assess the model's capability to capture TDI in the absence of turbulence. For flamelet-type models, this includes evaluating the choice of control variables and the mapping procedure from the lookup table.

Three cases with equivalence ratios of $\phi = 0.4$, $\phi = 0.6$, and $\phi = 0.8$ are considered for this configuration. The computational domains are square, with side lengths of $L = 0.08\text{m}$, $L = 0.052\text{m}$, and $L = 0.048\text{m}$, for $\phi = 0.4 - 0.8$, respectively. These correspond to more than 100 times the laminar unstretched flame thicknesses, $l_\text{F} = 714\mu\text{m}$, $l_\text{F} = 392\mu\text{m}$, and $l_\text{F} = 378\mu\text{m}$. With reference to Fig. 3, periodic boundary conditions are applied in the transverse (y) direction, while in the streamwise (x) direction, a uniform inflow boundary is prescribed at the bottom and an outflow boundary at the top of the computational domain.

At the inlet, an unburnt hydrogen-air mixture enters at ambient conditions, temperature $T = 298\text{K}$ and pressure $p = 1\text{atm}$, with a velocity U_x set equal to the precomputed consumption speeds $s_\text{c} = 0.65\text{m/s}$, $s_\text{c} = 1.5\text{m/s}$, and $s_\text{c} = 2.4\text{m/s}$ for $\phi = 0.4 - 0.8$, respectively, to ensure flame stabilization within the computational domain. Burnt gases exit the domain through the outlet. The simulations are initialized using one-dimensional unstretched flamelets, obtained from *FlameMaster* (Pitsch 1998) calculations, and placed in the middle of the domain aligned with the x-direction. To promote the development of TDI, the initially planar flame is perturbed with a harmonic perturbation of the form,

$$F(x) = A_0 \cdot \cos(ky)\,. \tag{1}$$

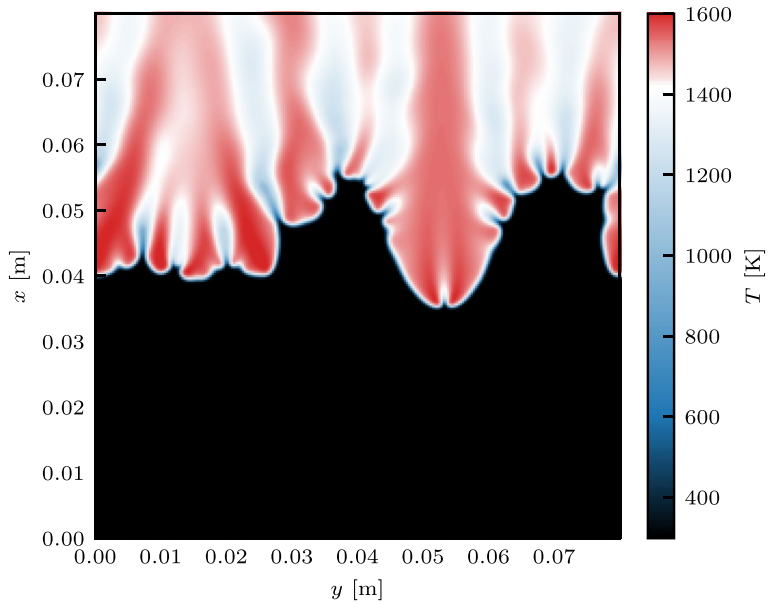


Fig. 3 Instantaneous T-field for the laminar, two-dimensional statistically planar flame test case with $\phi = 0.4$

The flame is resolved with approximately 14 grid points per laminar, unstretched flame thickness. The reference data were generated using the in-house solver *CIAO* (Desjardins et al. 2008), including a kinetic mechanism comprising 9 species and 46 reactions (Burke et al. 2012). The flamelets used for initialization are provided together with the validation data. A detailed description of the computational setup and numerical methods employed can be found in Desjardins et al. (2008) and Berger et al. (2022b).

Validation data include instantaneous temperature fields for a visual comparison of the flame structure and the super-adiabatic temperatures. Further, conditional means of a progress variable C, the progress variable source term $\bar{\dot{\omega}}_C$, and a mixture fraction Z (see Sect. 3.1) used in the flamelet model are included, as reported in Sect. 2.4.

2.1.2 RWTH Turbulent Slot Burner DNS

Three DNS of lean premixed hydrogen-air slot flames at varying Karlovitz numbers are considered (Berger et al. 2024; Gauding et al. 2026). The slot burner configuration is selected as it features a statistically planar flame with no mean curvature. Moreover, it provides access to fully-resolved three-dimensional fields of all transported quantities as well as derived statistical quantities. For this set of cases, it was shown that with increasing Karlovitz number, the effects of TDI first increase, then decrease. The latter occurs despite a further increase of the stretch factor I_0, because of a decrease in flame surface area, making this a challenging validation case (Berger et al. 2024). Because the Reynolds number is kept constant for the three cases, the slot burner data set enables an evaluation of TCI models under similar turbulence conditions, but varying turbulence-chemistry interactions. The cases will be denoted with K1, K2, and K3 from low to high Karlovitz number. The Karlovitz number for this configuration is defined as

$$Ka = \frac{t_\mathrm{F}}{t_\eta}, \tag{2}$$

where $t_\mathrm{F} = l_\mathrm{F}/s_\mathrm{L}$ is the chemical time scale, computed using the laminar unstretched burning velocity s_L, and $t_\eta = (\nu/\epsilon)^{1/2}$ is the Kolmogorov time scale, where ν is the kinematic viscosity and ϵ is the mean turbulent kinetic energy dissipation rate. The Karlovitz number was evaluated on the unburnt side of the flame using a hydrogen-based progress variable $C_{\mathrm{H_2}} = 0.1$, defined as

$$C_{\mathrm{H_2}} = 1 - \frac{Y_{\mathrm{H_2}}}{Y_{\mathrm{H_2,u}}}, \tag{3}$$

where $Y_{\mathrm{H_2}}$ is the mass fraction of hydrogen and the subscript "u" denotes values in the unburnt mixture. Ka is 20, 50, and 230 for the three cases K1, K2, and K3, respectively, calculated at approximately half the flame height. The jet Reynolds number, defined as

$$Re = \frac{U_\mathrm{ref} L_\mathrm{ref}}{\nu}, \tag{4}$$

is $Re = 11000$, where U_{ref} is the reference velocity corresponding to the bulk velocity at the slot inflow and L_{ref} is the characteristic length, which corresponds to the slot width H for the slot burner. The Karlovitz number variation is achieved by halving the slot width while doubling the bulk velocity in a way that the Reynolds number remains constant. For all the operating conditions considered, a laminar coflow consisting of combustion products at chemical equilibrium with an adiabatic temperature $T_{\mathrm{ad}} = 1415\mathrm{K}$ is used to stabilize the flames. The computational domain features free-slip boundary conditions in the cross-flow direction (y-axis) and periodic boundary conditions in the statistically homogeneous spanwise direction (z-axis). The premixed hydrogen-air inflow has an equivalence ratio of $\phi = 0.4$ at ambient conditions ($T = 298\mathrm{K}$ and $p = 1\mathrm{atm}$). An isosurface of the instantaneous hydrogen-based progress variable $C_{\mathrm{H_2}}$, colored by the heat release rate (HRR), is shown in Fig. 4 for the lowest Karlovitz-number case K1. The effects of TDI are evident from the formation of finger-like structures associated with locally increased heat release in regions convex towards the unburnt mixture, thereby highlighting the relevance of the present case for the validation framework.

The spatial resolutions for the three DNS cases K1, K2, and K3 are $\Delta_{\mathrm{K1}} = 70\mu\mathrm{m}$, $\Delta_{\mathrm{K2}} = 35\mu\mathrm{m}$, and $\Delta_{\mathrm{K3}} = 16.5\mu\mathrm{m}$, with corresponding domain sizes of $15H \times 10H \times 4.6H$, $30H \times 20H \times 4.45H$, and $45H \times 30H \times 8.4H$, respectively. The kinetic mechanism proposed by Burke et al. (2012) was employed, and simulations were performed using the

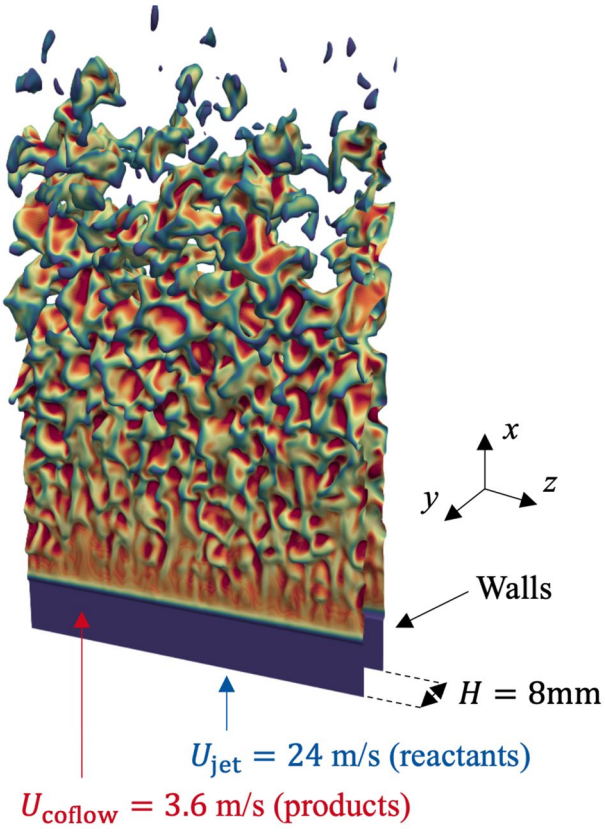


Fig. 4 Illustration of the turbulent slot burner DNS configuration depicting an isosurface of instantaneous progress variable $C_{\mathrm{H_2}}$, colored by HRR (increasing from blue over yellow to red) at $Re = 11000$ for case K1

in-house solver *CIAO* (Desjardins et al. 2008), with detailed descriptions of the numerical approach employed provided in Berger et al. (2024) and Gauding et al. (2026).

The validation data includes one full resolution (DNS) two-dimensional snapshot, as well as the corresponding box-filtered two-dimensional snapshot of the temperature field at several filter widths ($l_\mathrm{F}/\Delta_\mathrm{Filter} = 0.625, 1.25, 2.5, 5$). In addition, precomputed joint probability density functions (PDFs), conditional statistics, the turbulent flame surface area A_T, consumption speed s_c, and stretch factor I_0 are provided. All statistics have been obtained by averaging both in the z-direction and over time.

2.1.3 TU Darmstadt Piloted Turbulent Jet Burner Experiment

The TU Darmstadt piloted turbulent jet burner, experimentally investigated by Shi et al. (2024), is included in the validation framework. A schematic of the jet burner is shown in Fig. 5. In contrast to the slot burner configurations, the jet flame exhibits non-zero mean curvature along the entire flame brush and increased flame-flame interaction towards the flame tip. This aspect provides a useful test for assessing whether the model captures the influence of mean curvature on TDI.

The jet burner has a diameter of $L_\mathrm{ref} = D = 4.5\mathrm{mm}$ and is surrounded by a concentric pilot stream through a sintered burner plate with a porosity of 0.4. The jet Reynolds number, based on D, is $Re = 13820$. For this configuration, the Karlovitz number is defined as

$$Ka = \left(\frac{U'}{s_\mathrm{L}}\right)^{\frac{3}{2}} \frac{l_\mathrm{F}}{l_\mathrm{t}}, \tag{5}$$

where U' is the root-mean-square of the velocity fluctuations, and l_t is the integral length scale. The Karlovitz number, measured at a height $x/D = 7$ above the burner, is $Ka = 50$. U' was measured at the flame position with particle image velocimetry (PIV) and l_t was estimated as the half-width at half-maximum of the radial profile of the axial velocity. Additional details about the Karlovitz number calculation for this specific experimental setup can be found in Shi et al. (2024).

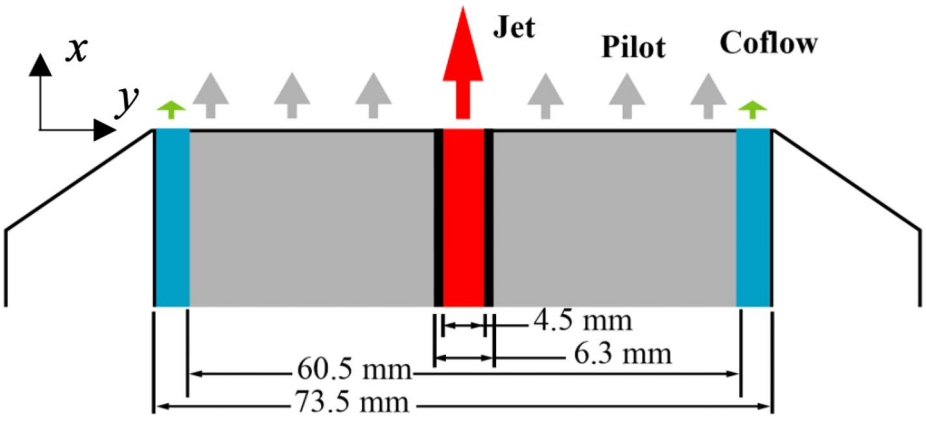


Fig. 5 Schematic of jet burner setup (Shi et al. 2024). Reprinted with permission from (Shi et al. 2024)

The premixed hydrogen-air stream has an equivalence ratio of $\phi = 0.4$ at ambient conditions ($T = 298\text{K}$ and $p = 1\text{atm}$) and a bulk jet inflow velocity of $U_{\text{ref}} = 50\text{m/s}$. The laminar pilot stream, employed to stabilize the flame, consists of equilibrium combustion products with an adiabatic temperature $T_{\text{ad}} = 1427\text{K}$. The coflow consists of N_2 injected at a constant flow velocity (1 m/s).

The validation dataset for this case includes high-spatial-resolution 1D and 2D optical measurements. Specifically, temperature profiles were obtained using 1D Rayleigh scattering, while species mole fractions of H_2, H_2O,O_2, and N_2 were measured using 1D Raman scattering. Additionally, 2D Rayleigh scattering snapshots captured the instantaneous flame structure. A detailed description of the experimental methods can be found in Shi et al. (2024). For validation purposes, the dataset includes a snapshot of the flame structure as well as the conditional means of the hydrogen mole fraction X_{H_2}, the water mole fraction X_{H_2O}, and the equivalence ratio ϕ as a function of temperature T.

2.1.4 NTNU Turbulent Bluff-Body Burner Experiment

A lean premixed turbulent hydrogen-air flame in the NTNU bluff-body burner configuration, experimentally investigated by Æsøy and Dawson (2024), is included in the validation framework. A schematic of this burner setup is shown in Fig. 6. In this configuration, the bluff-body generates a central recirculation zone that anchors the flame within the shear layers, thereby providing a fundamentally different flame stabilization mechanism compared to the jet and slot burner configurations.

The annular jet velocity is $U_{\text{ref}} = 20\text{m/s}$ at the nozzle exit, resulting in a Reynolds number of $Re = 17300$, based on the bluff-body diameter $L_{\text{ref}} = D = 13\text{mm}$. The Reynolds number based on the annular diameter at the nozzle exit $D_{\text{annulus}} = 6\text{mm}$ is $Re = 8000$.

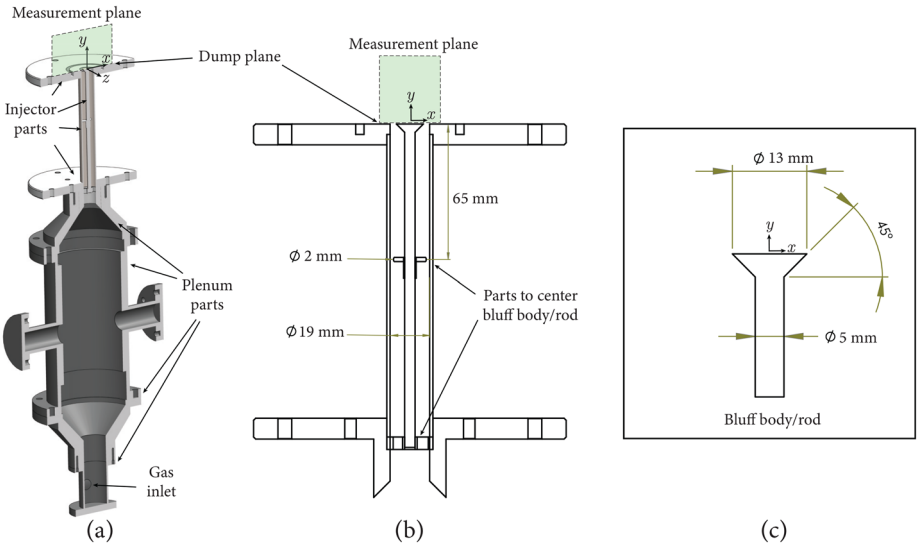


Fig. 6 Schematic of NTNU bluff-body burner setup (Æsøy and Dawson 2024). (**a**) Single-sector combustor, (**b**) injector pipe assembly, and (**c**) bluff-body/rod. Reprinted with permission from (Æsøy and Dawson 2024)

Although the Karlovitz number is not explicitly provided with the validation data, it can be estimated from the available data using an approach analogous to that employed for the jet burner, resulting in $Ka = 35$ at $x/D = 2.3$. The flame is unconfined and operates with no coflow or pilot stabilization, which distinguishes it from the aforementioned test cases. The premixed hydrogen-air stream has an equivalence ratio of $\phi = 0.4$ at ambient conditions ($T = 298\text{K}$ and $p = 1\text{atm}$).

For this validation case, both non-reacting and reacting velocity flow fields are available. Moreover, an estimate of the heat release q, derived from OH-chemiluminescence, is included. In addition, planar OH-PLIF provides spatially resolved intensity fields I at the bluff-body center plane, enabling characterization of flame structure and reaction-zone dynamics. A comprehensive description of the experimental diagnostics and data processing procedures is provided in Æsøy and Dawson (2024).

2.2 *OpenFOAM* Validation Setups

The *OpenFOAM* simulation setups corresponding to the eight validation cases are described in the following. The two-dimensional laminar configuration employs the same mesh and boundary conditions as the finite-rate chemistry simulation (Sect. 2.1.1). For each of the five three-dimensional turbulent cases, the entire LES setups are provided, including computational grids and turbulent inflows. For consistency, the x-axis is chosen as the streamwise direction in all configurations. In the flame region, the LES mesh uses a grid spacing of $\Delta = 280\mu\text{m}$, corresponding to approximately 2.5 grid points per laminar unstretched flame thickness. The mesh is gradually coarsened to $\Delta = 560\mu\text{m}$ away from the flame. For the different Karlovitz-number cases, the mesh size is adjusted to maintain a constant ratio between the LES and DNS grid resolutions. Simulations with coarser resolutions of $\Delta = 560\mu\text{m}$ and $\Delta = 1120\mu\text{m}$ in the flame region are included in the framework to facilitate systematic grid-sensitivity analyses of the LES model. Different grid resolutions can be easily generated using the provided meshing scripts.

The slot burner configuration is set up as a rectangular computational domain, with the *blockMesh* utility of *OpenFOAM*. Free-slip boundary conditions are applied in the lateral direction (y-axis), and periodic boundary conditions are imposed in the statistically homogeneous spanwise direction (z-axis).

For the jet and bluff-body burners, cylindrical computational domains are constructed using the *snappyHexMesh* utility due to their complex geometries. In these cases, free-slip boundary conditions are applied in the radial direction. The bluff-body burner domain comprises the upstream pipe section, including the embedded bluff-body.

Across all configurations, a premixed hydrogen-air mixture with an equivalence ratio of $\phi = 0.4$ enters at ambient conditions ($T = 298\text{K}$ and $p = 1\text{atm}$). The inflow is prescribed using the *timeVaryingMappedFixedValue OpenFOAM* boundary condition at the inlet. For the turbulent inflow data generation, the *CIAO* code has been used, which has been validated for different Reynolds numbers against the channel flow reference data by Moser et al. (1999). The inflow data was generated by performing a DNS of a fully developed turbulent flow per case in a periodic domain with pressure forcing applied to maintain a constant mean flow. The computational grid satisfies $y^+ < 1$ at the wall, while fully resolving the Kolmogorov length scale. Temporally sampled two-dimensional instantaneous planes of the velocity field were extracted to provide a realistic turbulent inflow for *OpenFOAM* and

are provided within the validation framework. The slot and the jet burner simulations are initialized with fully burnt products at equilibrium. In contrast, the bluff-body simulation is first run as a cold-flow case, after which the flame is ignited using a ring of fully burnt products. This is required to achieve the same flame structure as in the experiment. Alternatively, the simulations can be initialized with the instantaneous results of the provided LES, to reduce the time to convergence. The flow conditions and the main computational parameters, including the number of cells N_{cells} and the required computing time CPU-h, are summarized in Table 1, where the domain sizes L_x, L_y, and L_z are normalized by the characteristic length L_{ref} of each case. Here, the characteristic length is defined as the slot width H or the jet or bluff-body diameter D.

OpenFOAM solves the reactive Navier-Stokes equations in the low-Mach number limit along with scalar transport equations for the combustion model (see Sect. 3). The governing equations are discretized using a finite-volume formulation in conservative form. Time integration is performed using the implicit second-order *backward* scheme. Spatial discretization is performed using a second-order central differencing scheme (*Gauss linear*) for velocity, and a total-variation-diminishing (TVD) scheme (*Gauss limitedLinear 1*) for scalar transport. The TVD scheme was chosen due to its robustness and due to the lack of higher-order stability-preserving schemes suitable for scalar transport in the standard OpenFOAM distribution. These settings are used as a baseline setup, but can be readily modified or adjusted if alternative numerical schemes, available in *OpenFOAM*, are to be investigated. Furthermore, the user can adjust the output frequency and the solver tolerances as required.

The time step is dynamically adjusted according to the Courant–Friedrichs–Lewy (CFL) condition based on the local flow velocities, with a maximum allowed CFL number of 0.4. Each simulation is run for more than four flow-through times t_{Flow}, defined as $t_{\mathrm{Flow}} = L_x/U_{\mathrm{ref}}$. Statistical quantities are collected over two flow-through times once a statistically stationary state is reached.

Table 1 Computational setup of the (a) slot, (b) piloted jet, and (c) bluff-body LES configurations

	Slot			Piloted Jet	Bluff-Body
	K1	K2	K3		
H(mm)	8	4	2	-	-
D(mm)	-	-	-	4.5	13
U_{ref}(m/s)	24	48	96	50	20
U_{coflow}(m/s)	3.6	7.2	14.4	2.4	0
ϕ	0.4	0.4	0.4	0.4	0.4
$l_{\mathrm{F}}(\mu\mathrm{m})$	714	714	714	714	714
$\Delta(\mu\mathrm{m})$	560	280	140	280	280
$\Delta/\Delta_{\mathrm{DNS}}$	8	8	8	-	-
Re	11000	11000	11000	13820	17300
Ka	20	50	230	50	35
L_x/L_{ref}	17.5	35	70	30	8.46
L_y/L_{ref}	13	26	52	30	16.92
L_z/L_{ref}	4.55	4.2	8.4	30	16.92
N_{cells}	$1.8 \cdot 10^6$	$6.1 \cdot 10^6$	$48.4 \cdot 10^6$	$3.7 \cdot 10^6$	$8.8 \cdot 10^6$
CPU-h (h)	1536	6720	26880	11520	10560

2.3 Automatic Simulation Runner

Particularly in the context of machine learning, tools and approaches exist to automate many *OpenFOAM* simulations (Feng et al. 2025; Maric et al. 2025). While these approaches offer interesting opportunities for extending the framework to a large amount of cases, the current implementation relies on lightweight Python scripts to automate the simulation workflow, thereby maintaining minimal requirements on the user side.

As the framework is designed to provide a high degree of flexibility in terms of usability and adaptability, the user is required to specify only a limited set of parameters, depending on the particular model implementation. For example, scripts are provided to add boundary conditions for additional fields, if required, and to automatically include parameter variations. To execute the validation framework, the user defines the model to be evaluated, the corresponding model library to be loaded, the relevant SLURM parameters and the validation cases to be considered within the provided configuration file *config_main.yaml*. The Python control script *main.py* is then executed, which automatically starts the preprocessing, such as domain decomposition, then submits an individual SLURM job for each selected validation case using the parameters specified in the configuration file, performs the reconstruction of processor directories once the simulations are finalized using the *reconstructPar* utility, and finally starts the postprocessing, which is further discussed in Sect. 2.4.

Considering the "CLAIX-2023" computing cluster (CPU vendor: Intel Xeon 8468 Sapphire Rapid) at RWTH Aachen University, the validation cases require between 4 and 72 hours of wall-clock time, using four compute nodes with 96 tasks per node. The solver is parallelized with *decomposePar* utility from *OpenFOAM* with the *simple* decomposition method.

2.4 Postprocessing

To analyze the simulation output and compare it with the available validation data (see Sect. 2), a modular suite of Python postprocessing scripts is provided, to ensure consistent postprocessing for the performed simulations and the validation data. After completion of the simulations, the postprocessing script is executed by the main control script to perform data preparation steps, such as temporal averaging, and to invoke a set of modular routines that evaluate the agreement between the reference validation data and the LES results. This process is structured in three steps. In the first step, the required information is extracted from the LES and the validation data and it is made available for further processing. In the second step, the relevant quantities are computed, stored, and in a third step finally plotted. Storing the processed data enables the user to quickly adjust plotting settings if required. An example of the full postprocessing output is reported in the Supplementary Material, and some selected results are discussed in Sect. 4.

A summary of the provided validation data for the four configurations is given in Table 2. In the following, the global quantities evaluated during postprocessing are defined. Here, $\overline{\cdot}$ denotes the filtering operator, while $\widetilde{\cdot}$ represents density-weighted filtering. The normalized fuel flux $\mathcal{F}$ is defined as

Table 2 Summary of processed validation data for the (a) statistically planar, (b) slot, (c) piloted jet, and (d) bluff-body configurations

	Statistically Planar	Slot	Piloted Jet	Bluff-Body
Inst. slice in x-y-plane	T	$\widetilde{T}$	X_{OH}	X_{OH}
Avg. slice in x-y-plane	-	$\langle\widetilde{T}\rangle$	-	$\langle U_x\rangle, \langle U_y\rangle$
	$\langle Z\vert C\rangle$	$\langle\widetilde{Z}\vert\widetilde{C}\rangle$	$\langle\phi\vert T\rangle$	-
$\langle\cdot\vert\cdot\rangle$	$\langle\dot{\omega}_C\vert C\rangle$	$\langle\bar{\dot{\omega}}_C\vert\widetilde{C}\rangle$	$\langle X_{\mathrm{H_2}}\vert T\rangle$	-
			$\langle X_{\mathrm{H_2O}}\vert T\rangle$	-
Joint PDF$(\widetilde{Z},\widetilde{C})$	-	✓	-	-
Joint PDF$(\bar{\dot{\omega}}_C,\widetilde{C})$	-	✓	-	-
$A_{\mathrm{T}}, s_{\mathrm{c}}, I_0$	-	✓	-	-

$$\mathcal{F} = \frac{1}{\rho_{\mathrm{u}} U_{\mathrm{ref}} L_{\mathrm{ref}} Y_{\mathrm{H_2,u}}} \int \langle \bar{\rho}\widetilde{U}_x \widetilde{Y}_{\mathrm{H_2}} \rangle_{z,t} \, \mathrm{d}y \,, \tag{6}$$

for rectangular domains, where $\bar{\rho}$ is the filtered density, $\langle \dots \rangle_{z,t}$ denotes averaging over the periodic spatial direction and time. For cylindrical domains, the fuel flux is evaluated analogously, with averaging performed over the circumferential direction and integration carried out over the radial coordinate. To determine the turbulent flame surface area A_{T}, the instantaneous flame surface area A_{inst} defined by the isosurface $C_{\mathrm{H_2O}} = \widetilde{Y}_{\mathrm{H_2O}}/Y_{\mathrm{H_2O,b}} = 0.9$, is used. Note that the subscript "b" denotes quantities at chemical equilibrium. This evaluation is performed by time-averaging A_{T} for 50 ensembles using equally large regions along the streamwise direction. The isosurface extraction is carried out using the *PyVista* Python interface (Sullivan and Kaszynski 2019), which relies on the marching cubes algorithm. The consumption speed is calculated as (Poinsot and Veynante 2005)

$$s_{\mathrm{c}} = \frac{1}{\rho_{\mathrm{u}} A_0 Y_{\mathrm{H_2O,b}}} \int_{\mathcal{V}} \langle \bar{\dot{\omega}}_{\mathrm{H_2O}} \rangle_{\mathrm{t}} \, \mathrm{d}V \,, \tag{7}$$

where A_0 is the reference flame surface area, defined by the isosurface $\langle C_{\mathrm{H_2O}} \rangle_t = 0.9$ on the time-averaged progress variable field, $\overline{\dot{\omega}}_{\mathrm{H_2O}}$ is the resolved source term of the transport equation of water mass fraction, $Y_{\mathrm{H_2O}}$, and $\mathcal{V}$ denotes the bin volume. The stretch factor is defined as

$$I_0 = \frac{s_{\mathrm{c}}}{s_{\mathrm{L}}} \frac{A_0}{A_{\mathrm{T}}}. \tag{8}$$

The postprocessing framework is designed to be flexible and modular, allowing the user to specify which of the aforementioned quantities should be calculated. For further details, see Sect. 4.

3 Implemented Combustion Model

To demonstrate and validate the proposed framework, a state-of-the-art flamelet-based {LES combustion model for lean premixed hydrogen-air flames, developed by Berger et al. (2025), is implemented within the "Model Development" module. Although the model has shown promising capability in capturing TDI effects, it has only been applied to a single configuration. Next, the model formulation is briefly outlined, followed by a description of its implementation in *OpenFOAM*.

3.1 Model Formulation

The model proposed by Berger et al. (2025) is an extension of the work by Regele et al. (2013) and Schlup and Blanquart (2019) to account for turbulence-flame subfilter-scale interactions. The formulation involves transport equations for the progress variable, C, and a mixture fraction, Z, coupled with a tabulated chemistry database. The lookup table is constructed from a set of one-dimensional, unstretched premixed flames with varying equivalence ratios, where the thermochemical states are parameterized as functions of C and Z. Including the mixture fraction as a manifold coordinate has been shown to be essential to capture equivalence ratio fluctuations due to preferential diffusion (Regele et al. 2013). The model further accounts for the Soret effect, while a one-step chemistry assumption is adopted in deriving the mixture-fraction transport equation.

The model formulation employs a progress variable based on the water mass fraction (Berger et al. 2025), defined as

$$C = Y_{\mathrm{H_2O}}, \tag{9}$$

and the mixture fraction is defined according to Schlup and Blanquart (2019) and Berger et al. (2025) as

$$Z = \frac{\nu_{\mathrm{st}} Y_{\mathrm{H_2}} - Y_{\mathrm{O_2}} + Y_{\mathrm{O_2,air}}}{\nu_{\mathrm{st}} + Y_{\mathrm{O_2,air}}}, \tag{10}$$

where $\nu_{\mathrm{st}} = M_{\mathrm{O_2}}/2M_{\mathrm{H_2}}$, and $Y_{\mathrm{H_2}}$ and $Y_{\mathrm{O_2}}$ denote the local mass fractions of hydrogen and oxygen, respectively. $M_{\mathrm{O_2}}$ and $M_{\mathrm{H_2}}$ are the molar masses of oxygen and hydrogen, and $Y_{\mathrm{O_2,air}} = 0.233$ is the mass fraction of oxygen in the oxidizer. For the LES formulation, implicit filtering associated with the LES grid filter is assumed. The filtered transport equation for the progress variable is

$$\begin{aligned} &\frac{\partial}{\partial t}(\bar{\rho}\widetilde{C}) + \frac{\partial}{\partial x_j}(\bar{\rho}\widetilde{u}_j\widetilde{C}) = \bar{\dot{\omega}}_C \\ &+ \frac{\partial}{\partial x_j}\left(\bar{\rho}\widetilde{D}_C\frac{\partial \widetilde{C}}{\partial x_j}\right) + \frac{\partial}{\partial x_j}\left(\bar{\rho}\frac{\widetilde{D}_C^T}{\widetilde{T}}\frac{\partial \widetilde{T}}{\partial x_j}\right) - \frac{\partial}{\partial x_j}(\widetilde{\bar{\rho}u_jC} - \bar{\rho}\widetilde{u}_j\widetilde{C}), \end{aligned} \tag{11}$$

where $\bar{\dot{\omega}}_C$ is the filtered progress variable source term, D_C is the progress variable diffusion coefficient, and D_C^T is the diffusion coefficient for the Soret effect. The last term on the right-hand side corresponds to the subfilter scalar flux. In this approach, the correlations between

the diffusivity and the gradient of the progress variable and the temperature are neglected (Berger et al. 2025).

The filtered transport equation for the mixture fraction is given by

$$\begin{aligned}&\frac{\partial}{\partial t}(\bar{\rho}\tilde{Z}) + \frac{\partial}{\partial x_j}(\bar{\rho}\tilde{u}_j\tilde{Z}) = \frac{\partial}{\partial x_j}(\bar{\rho}\tilde{D}_Z\frac{\partial\tilde{Z}}{\partial x_j})\\ &-\frac{\partial}{\partial x_j}(\bar{\rho}\tilde{D}^*_Z\frac{\partial\tilde{C}}{\partial x_j}) + \frac{\partial}{\partial x_j}(\bar{\rho}\frac{\tilde{D}^T_Z}{\tilde{T}}\frac{\partial\tilde{T}}{\partial x_j}) - \frac{\partial}{\partial x_j}(\bar{\rho}\tilde{u}_j Z - \bar{\rho}\tilde{u}_j\tilde{Z}),\end{aligned} \tag{12}$$

where the diffusivities D_Z, D^*_Z and D^T_Z are defined according to Schlup and Blanquart (2019). The second term on the right-hand side accounts for preferential diffusion effects. The subfilter scalar fluxes are modeled based on the gradient-diffusion hypothesis. For the progress variable, this yields

$$-(\widetilde{\bar{\rho}u_jC} - \bar{\rho}\widetilde{u}_j\widetilde{C}) = \frac{\bar{\rho}\nu_\mathrm{t}}{Sc_\mathrm{t}}\frac{\partial\widetilde{C}}{\partial x_j}, \tag{13}$$

with the subgrid viscosity given by $\nu_\mathrm{t} = C_\mathrm{S}\Delta^2\sqrt{2\widetilde{S}_{ij}\widetilde{S}_{ij}}$ and the turbulent Schmidt number Sc_t set to 0.7. Here, C_S is the dynamic Smagorinsky coefficient determined with a test filter size of 2Δ, according to the procedure by Pierce and Moin (1998) using Lagrangian averaging (Meneveau et al. 1996), Δ is the filter width corresponding to the LES grid size, and $\widetilde{S}_{ij}$ is the filtered strain rate tensor based on $\widetilde{u}_i$ (Pope 2000). For the mixture fraction, the subfilter scalar flux is modeled similarly as

$$-(\widetilde{\bar{\rho}u_jZ} - \bar{\rho}\widetilde{u}_j\widetilde{Z}) = \frac{\bar{\rho}\nu_\mathrm{t}}{Sc_\mathrm{t}}\frac{\partial\widetilde{Z}}{\partial x_j}. \tag{14}$$

A presumed-PDF approach (Poinsot and Veynante 2005; Pitsch 2006) is employed to model the filtered progress variable source term (Berger et al. 2025), such as

$$\bar{\dot{\omega}}_C = \int \beta(C)\delta(\phi_\mathrm{Fl} - \hat{\phi}_\mathrm{Fl}) \cdot \dot{\omega}_C\,(C, \phi_\mathrm{Fl})\,\mathrm{d}C\mathrm{d}\phi_\mathrm{Fl}, \tag{15}$$

where the subfilter distribution of C is assumed to follow a β-PDF, while the flamelet index ϕ_Fl, defined as the nominal equivalence ratio of the flamelet used to generate the lookup table, is represented by a δ-PDF (Berger et al. 2025). The β-PDF formulation requires the variance of the progress variable C''^2, which acts as a third input parameter for the lookup table. This quantity is modeled following the dynamic approach of Pierce and Moin (1998) as

$$\widetilde{C''^2} = C_\mathrm{S}\Delta^2|\nabla\tilde{C}|^2. \tag{16}$$

3.2 Model Implementation in *OpenFOAM*

The model is implemented based on the *isothermalFluid* solver module in *OpenFOAM* version 11 Weller et al. (2023), named *fgmFluid*, and consists of three parts: a flexible lookup table reader, the model scalar transport equations, and an *OpenFOAM* thermophysical model class to handle the update of thermodynamic variables. Each component of *fgmFluid* serves as a template for the implementation of new models and can be reused. The temperature, density, diffusion coefficients, and the progress variable source term are retrieved from a lookup table using $\widetilde{C}$, $\widetilde{Z}$, and $\widetilde{C''^2}$ as input parameters. The table is generated using a set of 1D unstretched premixed flamelets with different global equivalence ratios $\phi \in [0.3, 1.0]$. The same kinetic mechanism used in the DNS proposed by Burke et al. (2012) has been used for lookup table generation. The implemented table reader accesses the lookup table by using a *tableProperties* file, specifying the table location, variables to read from the tables, and the input parameter names and grids. For laminar simulations, $\widetilde{C''^2}$ is set to zero in the model input file. Transport equations are solved for $\widetilde{C}$ and $\widetilde{Z}$ in the conservative form. The *PIMPLE* algorithm is employed with three outer correctors to couple the momentum and scalar transport. This number of outer correctors is required to ensure sufficient turbulence–chemistry coupling and, consequently, model accuracy.

4 Results and Discussion

This section presents the results obtained with the automated validation framework. The objective is twofold: first, to demonstrate the functionality and robustness of the framework, including its automated execution and postprocessing capabilities; and second, to assess the predictive performance of the implemented combustion model against reference data.

Visualizations of the turbulent inflow data are provided in the supplementary material to demonstrate that a sufficient range of turbulent scales is captured. Note that for the slot burner case, the same inflows have been used for LES and DNS. For each validation case, the framework automatically generates statistical quantities, conditional means, global flame metrics, and visual comparisons with the corresponding reference datasets. The following subsections discuss selected results for the individual configurations. The full output of the validation framework is attached in the supplementary material.

4.1 Two-Dimensional Laminar Statistically Planar Flame

The two-dimensional laminar statistically planar flames serve as baseline cases to assess the predictive capability of the implemented flamelet model in the absence of turbulence–chemistry interaction. The evaluation includes three operating conditions with $\phi = 0.4$, $\phi = 0.6$, and $\phi = 0.8$, introduced in Sect. 2.1.1, which exhibit different levels of TDI. Figures 7, 8, 9 show the conditional means $\langle Z|C\rangle$ and $\langle \dot{\omega}_C|C\rangle$ obtained from the *OpenFOAM* simulations within the validation framework, where the combustion model formulation introduced in Sect. 3 is employed.

The results are compared against the finite-rate chemistry reference solution obtained with the *CIAO* solver. The conditional mean $\langle Z|C\rangle$ is accurately reproduced across the entire range of the progress variable for case $\phi = 0.4$. For the two cases with higher equiva-

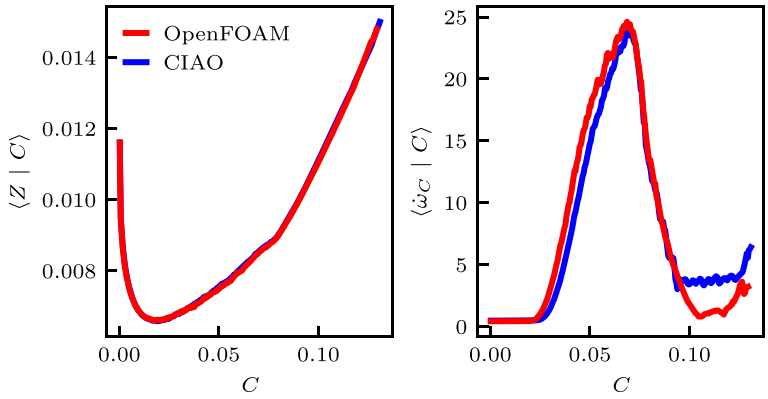


Fig. 7 Comparison of the conditional mean $\langle Z|C\rangle$ (left) and $\langle \dot{\omega}_C|C\rangle$ (right) between modeled results (*OpenFOAM*) and finite-rate chemistry data (*CIAO*) for the two-dimensional laminar statistically planar flame for case $\phi = 0.4$

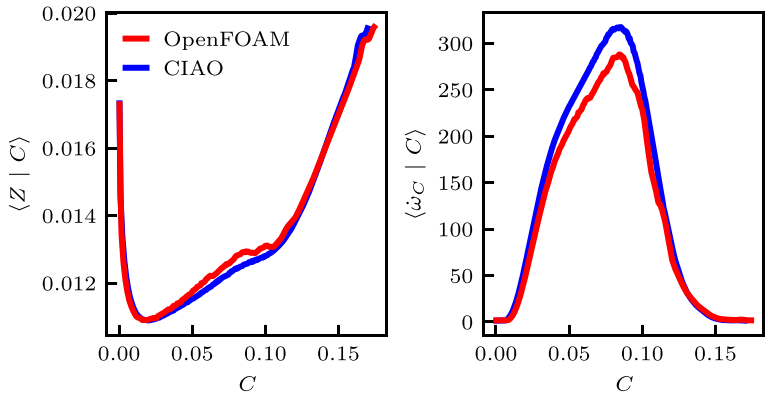


Fig. 8 Comparison of the conditional mean $\langle Z|C\rangle$ (left) and $\langle \dot{\omega}_C|C\rangle$ (right) between modeled results (*OpenFOAM*) and finite-rate chemistry data (*CIAO*) for the two-dimensional laminar statistically planar flame for case $\phi = 0.6$

lence ratios a slight over-prediction for medium progress variable values is observed. A slight under-prediction of the source term $\langle \bar{\dot{\omega}}_C|C\rangle$ is visible for super-equilibrium progress-variable values for case $\phi = 0.4$, while an under-prediction of the progress variable source term is observed for the cases $\phi = 0.6$ and $\phi = 0.8$. Overall, the global consumption speeds, reported in Table 3, match closely. The model yields a maximum deviation of approximately 5% for case $\phi = 0.4$. With this baseline case, the validation framework facilitates the evaluation of the model performance in different flame regions.

4.2 RWTH Turbulent Slot Burner

The LES results for the turbulent slot burner are compared to the filtered DNS data to assess the performance of the TDI model. For the DNS data, a box filter with a filter size of eight grid cells is used to match the LES filter. First, instantaneous $\widetilde{T}$-fields on an x-y-plane

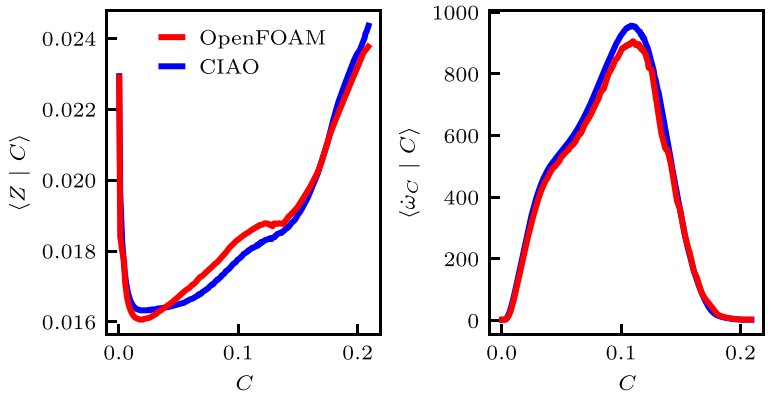


Fig. 9 Comparison of the conditional mean $\langle Z|C \rangle$ (left) and $\langle \dot{\omega}_C|C \rangle$ (right) between modeled results (*OpenFOAM*) and finite-rate chemistry data (*CIAO*) for the two-dimensional laminar statistically planar flame for case $\phi = 0.8$

Table 3 Summary of consumption speeds for the (a) $\phi = 0.4$, (b) $\phi = 0.6$, (c) $\phi = 0.8$ case

	$\phi = 0.4$	$\phi = 0.6$	$\phi = 0.8$
$s_{c,\text{model}}$	0.59 m/s	1.42 m/s	2.41 m/s
$s_{c,\text{ref}}$	0.62 m/s	1.48 m/s	2.45 m/s

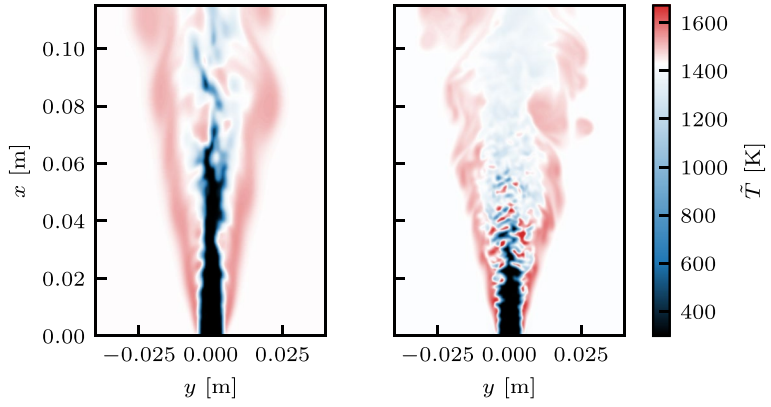


Fig. 10 Instantaneous $\widetilde{T}$-field on an x-y-plane for the LES (left) and the filtered DNS (right) for case K1

obtained from the LES (left) and the filtered DNS data (right) are compared in Figs. 10, 11, 12 for the three cases K1, K2, and K3, respectively. The comparison shows that the LES flamelet model captures the main qualitative features of the turbulent premixed hydrogen–air flames, including super-adiabatic temperatures and flame wrinkling. However, noticeable qualitative differences are observed in the flame length and the small-scale wrinkling of the LES flame surface compared to the filtered DNS.

For a quantitative comparison of the flame length, the axial fuel flux $\mathcal{F}$, is shown in Fig. 13. Interestingly, the consumption speeds of the DNS and the resulting flame lengths are independent of the Karlovitz number. This is consistent with the observations of Berger

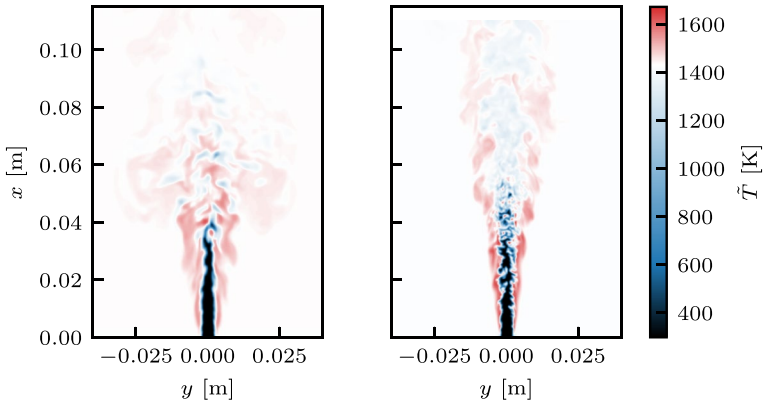


Fig. 11 Instantaneous $\widetilde{T}$-field on an x-y-plane for the LES (left) and the filtered DNS (right) for case K2

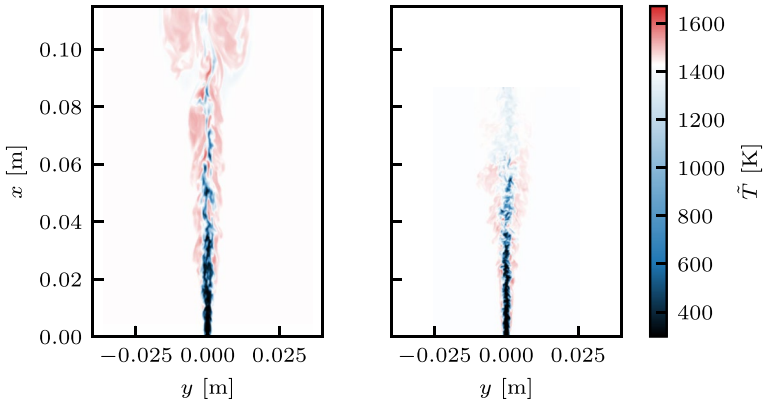


Fig. 12 Instantaneous $\widetilde{T}$-field on an x-y-plane for the LES (left) and the filtered DNS (right) for case K3

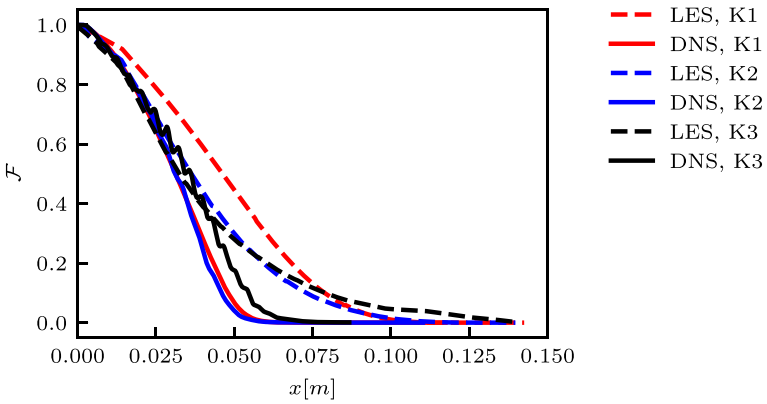


Fig. 13 Fuel flux for the LES (dashed lines) and the filtered DNS (solid lines) for all three Karlovitz number cases K1, K2, and K3

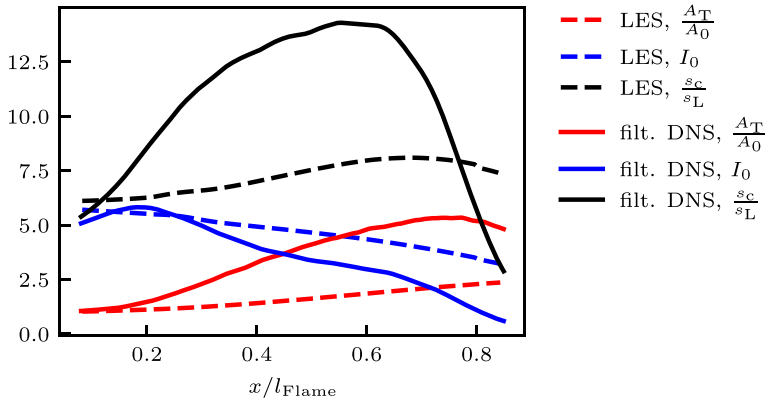


Fig. 14 Comparison of A_{T}/A_0, I_0, and $s_{\mathrm{c}}/s_{\mathrm{L}}$ between the LES and the filtered DNS along the normalized flame length for case K1

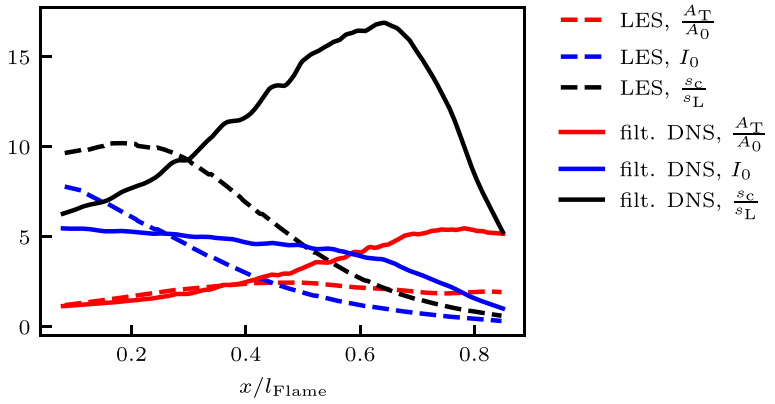


Fig. 15 Comparison of A_{T}/A_0, I_0, and $s_{\mathrm{c}}/s_{\mathrm{L}}$ between the LES and the filtered DNS along the normalized flame length for case K2

et al. (2024) and can be attributed to a compensation between reduced surface wrinkling and increased reactivity. This is different for the K1-case LES, mostly because of the lack of flame surface generation close to the nozzle. The flame length is over-predicted for all three Karlovitz number cases by approximately 30%. For cases K2 and K3, the differences are mostly in the downstream region of the flame.

To exemplarily show a further investigation of the observed differences, A_{T}/A_0, I_0, and $s_{\mathrm{c}}/s_{\mathrm{L}}$ along the streamwise coordinate are compared in Figs. 14, 15, 16 for K1–K3. Note that the grid size and hence the resolution of the laminar unstretched flame thickness increases from $l_{\mathrm{F}}/\Delta_{\mathrm{filtered}} = 1.25$ (K1), over $l_{\mathrm{F}}/\Delta_{\mathrm{filtered}} = 2.5$ (K2) to $l_{\mathrm{F}}/\Delta_{\mathrm{filtered}} = 5$ (K3). In the supplementary material, an investigation of different grid resolutions is presented. For case K1, A_{T} is systematically under-predicted by the LES, while I_0 is partly over-predicted, resulting in an overall under-prediction of the global consumption speed. This behavior is consistent with the over-prediction of the flame length and the reduced flame-wrinkling in the LES compared to the filtered DNS. For cases K2 and K3, a very

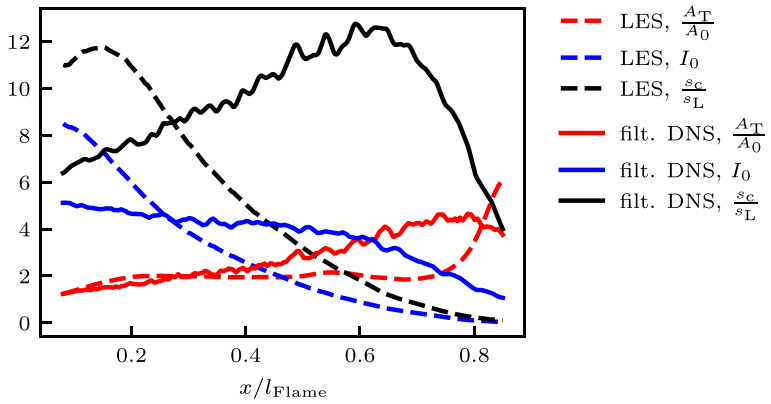


Fig. 16 Comparison of A_{T}/A_0, I_0, and $s_{\mathrm{c}}/s_{\mathrm{L}}$ between the LES and the filtered DNS along the normalized flame length for case K3

good prediction of A_{T} is observed in the nozzle-near region, where also the fuel flux is well predicted, while the predicted I_0 decreases much too strongly in downstream direction, which, as a consequence, leads to an under-prediction of the flame surface. This indicates an incorrect dependence of the model performance on the turbulence intensity at the flame scale. These results highlight the importance of evaluating models under varying operating conditions, as provided by the present validation framework.

Finally, to investigate the local flame state, the joint PDF of $\widetilde{Z}$ (left) and $\bar{\dot{\omega}}_C$ (right) conditioned on $\widetilde{C}$, respectively, are compared in Fig. 17. Overall, the mixture fraction distributions are in good agreement with the filtered DNS, with only minor deviations at the highest progress variable values. In case K3, the model correctly captures the significant reduction of ultra-lean regions compared to K1 and K2, indicating a consistent response to increasing turbulence intensity. The source term, however, is slightly under-predicted across the entire range of C, specifically for case K3. One possible explanation is the use of a lower-order numerical scheme for scalar transport in *OpenFOAM*, which may lead to partially under-resolved scalar gradients. This can reduce the variance of the progress variable and, consequently, the modeled source term. The results therefore suggest a potential sensitivity of the model performance to the order of the numerical scheme, which has to be further investigated, when higher-order scalar schemes are available in OpenFOAM. The validation framework includes the presented statistics to assess the accuracy with which the control variables and, thereby, the local flame state, are captured and whether the turbulence-chemistry interaction is predicted accurately.

In summary, validation against turbulent flames spanning different Karlovitz numbers is important for evaluating a model's performance to reliably predict varying turbulence-chemistry interaction mechanisms. The validation framework integrates the evaluation of global and local flame properties to systematically identify model strength and limitations and provide insight into their underlying causes.

4.3 TU Darmstadt Piloted Turbulent Jet Burner

LES results for the piloted turbulent jet burner are compared to the experimental data described in Sect. 2.1.3. Figure 18 shows a snapshot of the instantaneous mole fraction of

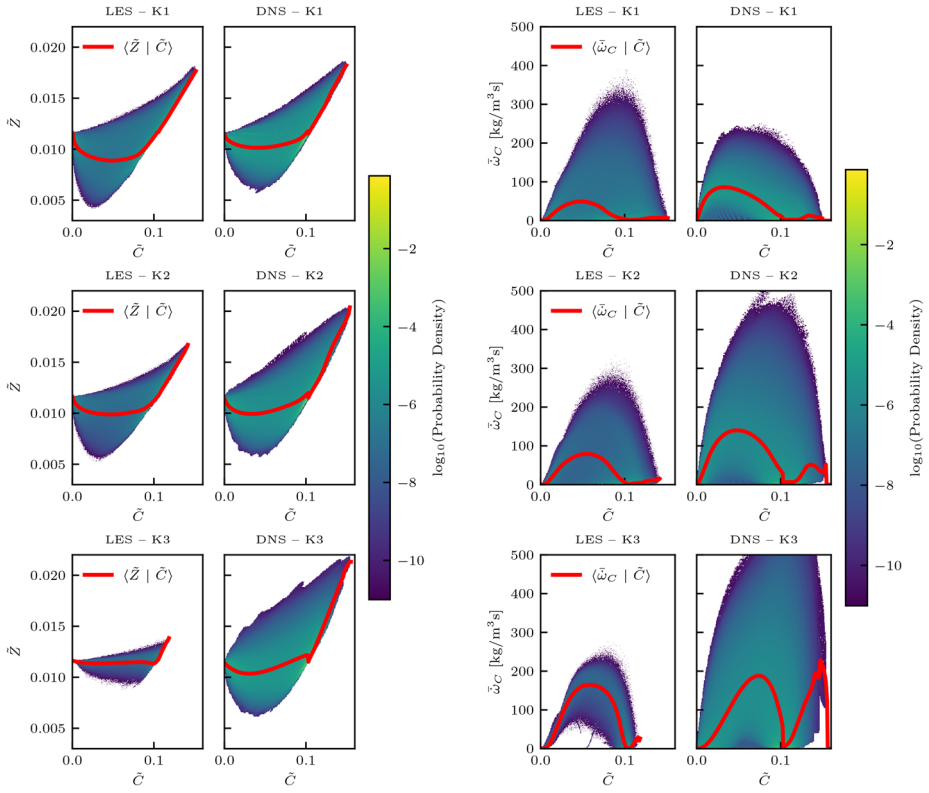


Fig. 17 Joint PDF of $\widetilde{Z}$ conditioned on $\widetilde{C}$ (left) and $\bar{\tilde{\omega}}_C$ conditioned on $\widetilde{C}$ (right) for the LES and the filtered DNS for cases K1, K2, and K3. Red lines represent the conditional mean

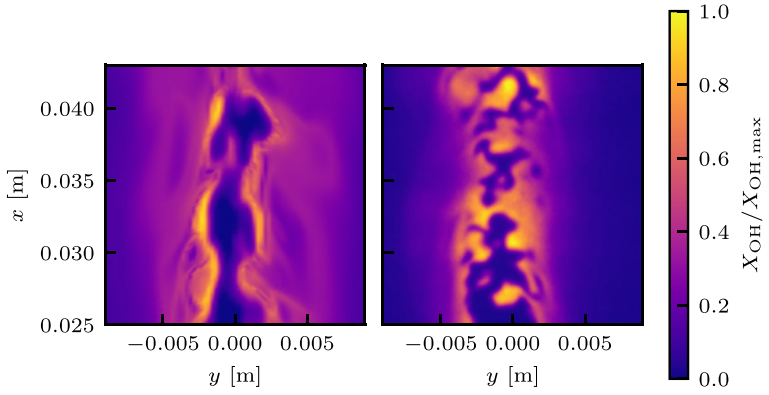


Fig. 18 Comparison of instantaneous normalized X_{OH} between the LES (left) and the experiment (right)

OH, X_{OH}, normalized by its peak value. The normalization ensures that the intensity from the OH-LIF measurements is qualitatively comparable to the LES result. It should be noted that the comparability between the LES results and the experimental data is limited due to the fact that the experimental data employ a different resolution and cannot be Favre filtered, because the density field is not available. Consequently, the comparison is not intended to demonstrate quantitative agreement, but rather to assess whether the LES reproduces the overall flame topology and structural features. The visual comparison indicates that the wrinkling of the flame is underestimated in the LES. This behavior is consistent with observations made for the turbulent slot flame simulations, suggesting a systematic tendency of the model to predict reduced small-scale flame surface wrinkling.

To further analyze the prediction of the flame structure, the conditional means $\langle X_{\mathrm{H_2}}|T\rangle$, $\langle X_{\mathrm{H_2O}}|T\rangle$, and $\langle\phi|T\rangle$ for the LES and the experimental data are compared in Fig. 19. Overall, the conditional means obtained from LES agree with the experimental data within the measurement uncertainty. However, the LES does not fully capture the highest temperature levels and, consequently, the largest progress variable values. This behavior may be linked to a slight under-prediction of the progress variable source term, consistent with the trends observed in the turbulent slot burner cases.

4.4 NTNU Turbulent Bluff-Body Burner

The bluff-body burner configuration tests the model under complex, recirculating flow conditions. Figure 20 shows a comparison of instantaneous normalized X_{OH} snapshots between the LES and the experimental data. The flame wrinkling is under-predicted in the LES, consistent with the observations for the slot and the jet burner simulations. The flame

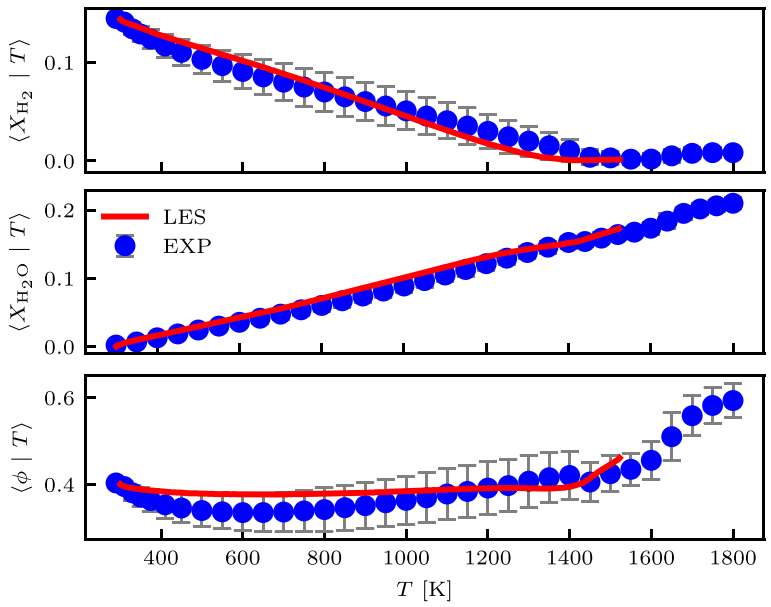


Fig. 19 Comparison of the conditional means $\langle X_{\mathrm{H_2}}|T\rangle$, $\langle X_{\mathrm{H_2O}}|T\rangle$, and $\langle\phi|T\rangle$ between LES and experimental data, where the error bars represent the standard deviation

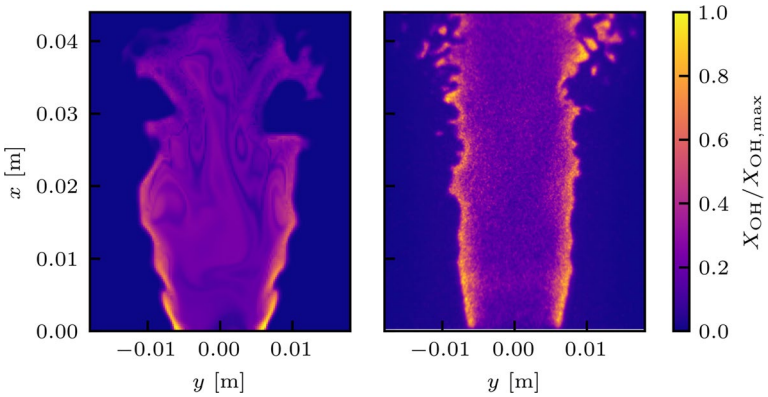


Fig. 20 Comparison of instantaneous normalized X_{OH} between the LES (left) and the experiment (right)

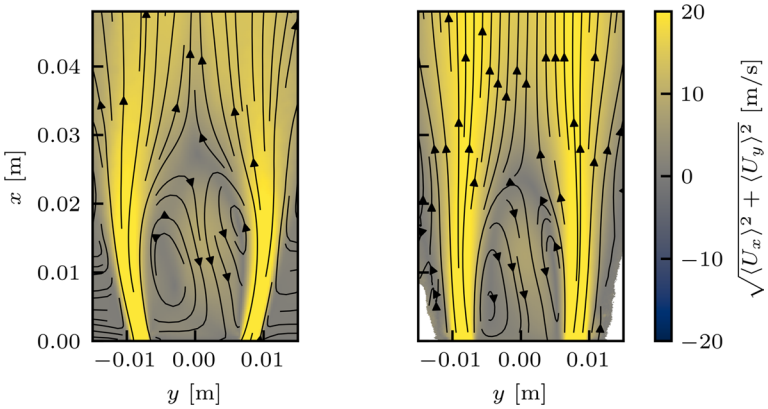


Fig. 21 Comparison of averaged velocity magnitude $\sqrt{\langle U_x\rangle^2 + \langle U_y\rangle^2}$ for a slice in the x-y-plane between the LES (left) and the experimental data (right)

shape in the LES differs slightly from the experiment, with the simulated flame being wider, possibly owing to differences in entrainment and turbulent mixing.

Figure 21 shows a comparison of the corresponding flow structure between the LES and the experimental data. The simulation captures the general topology of the flow field, including the formation of the central recirculation zone and the surrounding shear layers. Furthermore, both the magnitude of the velocity and the length of the recirculation zone are well predicted in the LES compared to the experimental measurements. However, the recirculation region is slightly wider in the simulation, indicating differences in the predicted momentum exchange and mixing processes.

For a quantitative assessment, radial velocity profiles at selected axial locations, covering the axial extent of the recirculation region observed in the experiment, are presented in Fig. 22. While the overall shape of the profiles is reasonably well reproduced, the LES slightly over-predicts the rate of flow recovery downstream of the bluff-body. This behavior is consistent with the wider recirculation zone observed in the mean flow fields and may be

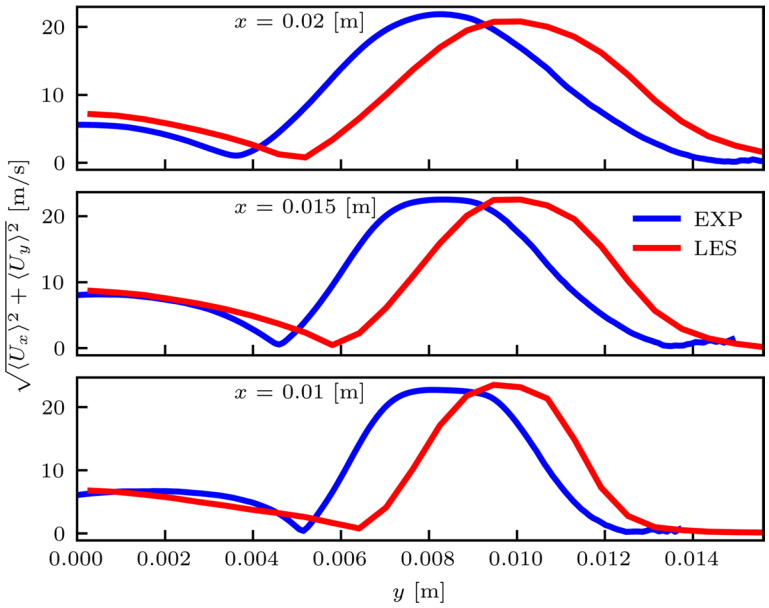


Fig. 22 Comparison of averaged velocity magnitude $\sqrt{\langle U_x \rangle^2 + \langle U_y \rangle^2}$ for three lines at heights $x = 0.01$ (bottom), $x = 0.015$ (middle), and $x = 0.02$ (top) between the LES and the experimental data

attributed to several factors. One possible reason is an overestimation of the turbulent mixing and the shear-layer growth, which can increase momentum transfer from the outer flow into the wake region. Overall, these results demonstrate that it is essential to analyze the flow field and combustion characteristics simultaneously, as inaccuracies in the predicted flow field directly affect flame stabilization, mixing, and heat release.

5 Conclusions

This work presents a validation framework for combustion models based on the open-source *OpenFOAM* CFD toolbox. The validation framework comprises eight representative cases, ranging from three two-dimensional laminar statistically planar flames to five three-dimensional turbulent flames, including three slot burner cases, a jet burner case, and a bluff-body burner case. This setup provides a starting point for a broad coverage of flow and combustion regimes to assess an LES model's performance for premixed hydrogen applications, specifically targeting TDI. To demonstrate its capabilities, the framework was applied to a state-of-the-art flamelet model for TDI, thereby providing, for the first time, a systematic assessment of its strengths and limitations under a broader range of conditions. The proposed framework provides a complete workflow, including tools and data for a rigorous validation of combustion models implemented in *OpenFOAM*. The code is modular and serves as a template for future model implementations added by the user. It establishes a baseline that can be extended to additional cases, operating conditions, and configurations in the future. Furthermore, it provides a tool for unifying efforts on modeling complex hydro-

gen flames and standardizing model assessment under well-defined conditions, giving clear insights into the strengths and deficiencies of each model.

Supplementary Information The online version contains supplementary material available at https://doi.org/10.1007/s10494-026-00745-z.

Acknowledgements SN, MG and HP gratefully acknowledge the funding from the Deutsche Forschungsgemeinschaft (DFG) Priority Program 2419 HyCAM (ID: 523874889) and the support from DFG within the project (ID: 516338899) IRTG 2983 Hy-Potential. LN and MV have received funding from the German Federal Ministry of Education and Research (BMBF) and the State of North Rhine-Westphalia as part of the NHR funding initiative. Further, the authors gratefully acknowledge the Gauss Centre for Supercomputing e.V. (https://www.gauss-centre.eu) for funding this project by providing computing time on the GCS Supercomputer SuperMUC-NG at Leibniz Supercomputing Centre Garching/LRZ, https://www.lrz.de. Finally, the authors gratefully acknowledge the computing time provided to them at the NHR Center NHR4CES at RWTH Aachen University (project number: p0025970). This is funded by the Federal Ministry of Education and Research, and the state governments participating on the basis of the resolutions of the GWK for national high-performance computing at universities (https://www.nhr-verein.de/unsere-partner).

Author contributions Conceptualization and Methodology: SN, MG, HP; Formal analysis and investigation: SN, LN, MV, MG; Writing - original draft preparation: SN; Writing - review and editing: LN, MV, MG, HP; Funding acquisition and Supervision: MG, HP.

Funding Open Access funding enabled and organized by Projekt DEAL.

Data availability The flamelet model code is available at https://gitlab.git.nrw/rwth-itv-public/openfoam-fgmfluid. The validation framework, including the setups and postprocessing scripts, and the link to the reference data for the validation framework are provided at https://gitlab.git.nrw/rwth-itv-public/combustion-model-validation-framework-openfoam.https://rwth-aachen.sciebo.de/s/HfWLbenDs7LdA4Q

Declarations

Competing interests The authors declare no competing interests.

Open Access This article is licensed under a Creative Commons Attribution 4.0 International License, which permits use, sharing, adaptation, distribution and reproduction in any medium or format, as long as you give appropriate credit to the original author(s) and the source, provide a link to the Creative Commons licence, and indicate if changes were made. The images or other third party material in this article are included in the article's Creative Commons licence, unless indicated otherwise in a credit line to the material. If material is not included in the article's Creative Commons licence and your intended use is not permitted by statutory regulation or exceeds the permitted use, you will need to obtain permission directly from the copyright holder. To view a copy of this licence, visit http://creativecommons.org/licenses/by/4.0/.

References

Æsøy, E., Dawson, J.R.: Dataset: A turbulent bluff-body stabilised H2-flame. https://tnfworkshop.org/bluff-body-hydrogen-flame-ntnu-trondheim/ (2024). Accessed January 2026

Aniello, A., Laera, D., Berger, L., Attili, A., Poinsot, T.: Introducing thermodiffusive effects in large-eddy simulation of turbulent combustion for lean hydrogen-air flames. In: Center for Turbulence Research, Proceedings of the Summer Program, pp. 267–277. (2022)

Aniello, A., Laera, D., Marragou, S., Magnes, H., Selle, L., Schuller, T., Poinsot, T.: Experimental and numerical investigation of two flame stabilization regimes observed in a dual swirl H2-air coaxial injector. Combust. Flame **249**, 112595 (2023)

Aniello, A., Poinsot, T., Selle, L., Schuller, T.: Hydrogen substitution of natural-gas in premixed burners and implications for blow-off and flashback limits. Int. J. Multiling. Hydrogen Energy **47**(77), 33067–33081 (2022)

Aspden, A., Howarth, T., Hunt, E.: Three-dimensional phenomenology of freelypropagating thermodiffusively-unstable lean premixed hydrogen flames. Proc. Combust. Inst. **40**(1–4), 105634 (2024)
Bae, J., Chaib, O., Weller, L., Moitro, A., Hunt, E.F., Aspden, A.J., Hochgreb, S.: Simultaneous imaging of OH and temperature in lean premixed hydrogen/air flames: which marker for thermodiffusive instability? (2025)
Barlow, R.: International workshop on measurement and computation of turbulent flames. https://tnfworkshop.org/hydrogen-flames/ (2024). Accessed January 2026
Barlow, R., Frank, J., Karpetis, A., Chen, J.-Y.: Piloted methane/air jet flames: transport effects and aspects of scalar structure. Combust Flame **143**(4), 433–449 (2005)
Barlow, R.S., Frank, J.H.: Effects of turbulence on species mass fractions in methane/air jet flames. In: Symposium (international) on Combustion, vol. 27, pp. 1087–1095. Elsevier (1998)
Berger, L., Attili, A., Gauding, M., Pitsch, H.: Effects of Karlovitz number variations on thermodiffusive instabilities in lean turbulent hydrogen jet flames. Proc. Combust. Inst. **40**(1–4), 105219 (2024)
Berger, L., Attili, A., Gauding, M., Pitsch, H.: LES combustion model for premixed turbulent hydrogen flames with thermodiffusive instabilities: a priori and a posteriori analysis. J. Fluid Mech. **1003**, 33 (2025)
Berger, L., Attili, A., Pitsch, H.: Intrinsic instabilities in premixed hydrogen flames: parametric variation of pressure, equivalence ratio, and temperature. Part 1 - dispersion relations in the linear regime. Combust. Flame **240**, 111935 (2022a)
Berger, L., Attili, A., Pitsch, H.: Intrinsic instabilities in premixed hydrogen flames: parametric variation of pressure, equivalence ratio, and temperature. Part 2 – nonlinear regime and flame speed enhancement. Combust. Flame **240**, 111936 (2022b)
Berger, L., Attili, A., Pitsch, H.: Synergistic interactions of thermodiffusive instabilities and turbulence in lean hydrogen flames. Combust. Flame **244**, 112254 (2022c)
Berger, L., Grinberg, M., Jürgens, B., Lapenna, P.E., Creta, F., Attili, A., Pitsch, H.: Flame fingers and interactions of hydrodynamic and thermodiffusive instabilities in laminar lean hydrogen flames. **39**(2), 1525–1534 (2023)
Burke, M.P., Chaos, M., Ju, Y., Dryer, F.L., Klippenstein, S.J.: Comprehensive H2/O2 kinetic model for high-pressure combustion. Int. J. Soc. Res. Methodol. Chem. Kinet. **44**(7), 444–474 (2012)
Calder, A.C., Fryxell, B., Plewa, T., Rosner, R., Dursi, L., Weirs, V., Dupont, T., Robey, H., Kane, J., Remington, B., et al.: On validating an astrophysical simulation code. Astrophys. J., Suppl. Ser. **143**(1), 201 (2002)
Calder, A.C., Townsley, D.M.: In: Beisbart, C., Saam, N.J. (eds.) Astrophysical Validation, pp. 685–709. Springer, Cham (2019)
Chung, W.T., Ihme, M., Jung, K.S., Chen, J.H., Guo, J., Brouzet, D., Talei, M., Jiang, B., Savard, B., Poludnenko, A.Y., Akoush, B., Sharma, P., Tamkin, A., Wang, Q., Shahane, S., Yifan, C., Coulon, V., Lapeyre, C.J.: BLASTNet Simulation Dataset. Zenodo (2024). https://doi.org/10.5281/zenodo.10732791
Day, M., Bell, J., Bremer, P.-T., Pascucci, V., Beckner, V., Lijewski, M.: Turbulence effects on cellular burning structures in lean premixed hydrogen flames. Combust. Flame **156**(5), 1035–1045 (2009)
Desjardins, O., Blanquart, G., Balarac, G., Pitsch, H.: High order conservative finite difference scheme for variable density low mach number turbulent flows. J. Comput. Phys. **227**(15), 7125–7159 (2008)
Dillon, S., Mercier, R., Fiorina, B.: Modelling turbulent multi-regime combustion in LES with filtered tabulated chemistry. Combust. Flame **286**, 114802 (2026)
Eu, E.: The European green deal. European Commission. https://commission.europa.eu/strategy-and-policy/priorities-2019-2024/european-green-deal_en (2019). Accessed January 2026
Feng, J., Xu, R., Chu, X.: OpenFOAMGPT 2.0: end-to-end, trustworthy automation for computational fluid dynamics. arXiv preprint arXiv:2504.19338 (2025)
Gauding, M., Berger, L., Pitsch, H.: Tnftarget flame: lean premixed turbulent hydrogen-air slot-jet flames at various Reynolds and Karlovitz numbers. https://tnfworkshop.org/workshop-proceedings/tnf16-workshop/ (2026). Accessed January 2026
Howarth, T., Day, M.S., Pitsch, H., Aspden, A.: Thermal diffusion, exhaust gas recirculation and blending effects on lean premixed hydrogen flames. Proc. Combust. Inst. **40**(1–4), 105429 (2024)
Howarth, T., Hunt, E., Aspden, A.: Thermodiffusively-unstable lean premixed hydrogen flames: phenomenology, empirical modelling, and thermal leading points. Combust. Flame **253**, 112811 (2023)
Hunt, E., Aspden, A.: Thermodiffusively-unstable lean premixed hydrogen flames: length scale effects and turbulent burning regimes. Combust. Flame **272**, 113855 (2025)
Im, H.G., Chen, J.H.: Preferential diffusion effects on the burning rate of interacting turbulent premixed hydrogen-air flames. Combust. Flame **131**(3), 246–258 (2002
Kanov, K., Burns, R., Lalescu, C., Eyink, G.: The johns hopkins turbulence databases: an open simulation laboratory for turbulence research. Comput. Sci. Eng. **17**(5), 10–17 (2015)

Lapenna, P.E., Berger, L., Creta, F., Pitsch, H.: Hydrogen laminar flames. In: Hydrogen for Future Thermal Engines, pp. 93–139. Springer, Cham (2023)
Lapenna, P.E., Troiani, G., D'Alessio, F., Creta, F.: Modeling aspects of thermodiffusively unstable turbulent premixed flames. Proc. Combust. Inst. **41**, 105963 (2025)
Li, T., Chen, H., Hochgreb, S.: Three-dimensional structure and burning speed of turbulent premixed H2–air and H2/CH4–air bunsen flames using high-speed tomographic imaging. Proc. Combust. Inst. **41**, 105830 (2025)
Mao, Y.-Y., Kovacs, E., Heitmann, K., Uram, T.D., Benson, A.J., Campbell, D., Cora, S.A., DeRose, J., Di Matteo, T., Habib, S., et al.: DESCQA: an automated validation framework for synthetic sky catalogs. Astrophys. J., Suppl. Ser. **234**(2), 36 (2018)
Maric, T., Fadeli, M.E., Rigazzi, A., Shao, A., Weiner, A.: Combining machine learning with computational fluid dynamics using openFoaM and Smartsim. Meccanica **60**(6), 1831–1850 (2025)
Marragou, S., Magnes, H., Aniello, A., Guiberti, T., Selle, L., Poinsot, T., Schuller, T.: Modeling of H2/air flame stabilization regime above coaxial dual swirl injectors. Combust. Flame **255**, 112908 (2023)
Meneveau, C., Lund, T.S., Cabot, W.H.: A Lagrangian dynamic subgrid-scale model of turbulence. J. Fluid Mech. **319**, 353–385 (1996)
Moser, R.D., Kim, J., Mansour, N.N., et al.: Direct numerical simulation of turbulent channel flow up to re= 590. Phys. Fluids **11**(4), 943–945 (1999)
Pérez-Sánchez, E.J., Fortes, E., Mira, D.: Assessment of the flamelet generated manifold method with preferential diffusion modeling for partially premixed hydrogen flames. Combust. Flame **277**, 114141 (2025)
Pierce, C.D., Moin, P.: A dynamic model for subgrid-scale variance and dissipation rate of a conserved scalar. Phys. Fluids **10**(12), 3041–3044 (1998)
Pitsch, H.: A C++ program package for 0D combustion and 1D laminar flames. (1998)
Pitsch, H.: Large-eddy simulation of turbulent combustion. Annu. Rev. Fluid Mech. **38**(1), 453–482 (2006)
Pitsch, H.: The transition to sustainable combustion: hydrogen- and carbon-based future fuels and methods for dealing with their challenges. Proc. Combust. Inst. **40**(1–4), 105638 (2024)
Pitsch, H., Trisjono, P.: Can combustion models be developed from DNS data. In: 19th Australasian Fluid Mechanics Conference, vol. 350, pp. 1–8. (2014)
Poinsot, T., Veynante, D.: Theoretical and Numerical Combustion. RT Edwards, Inc, Philadelphia, USA (2005)
Pope, S.B.: Turbulent Flows. Cambridge University Press, Cambridge, UK (2000)
Ramirez, F.A.M., Douasbin, Q., Dounia, O., Vermorel, O., Jaravel, T.: Flameturbulence interactions in lean hydrogen flames: implications for turbulent flame speed and fractal modelling. Combust. Flame **273**, 113926 (2025)
Regele, J.D., Knudsen, E., Pitsch, H., Blanquart, G.: A two-equation model for nonunity Lewis number differential diffusion in lean premixed laminar flames. **160**(2), 240–250 (2013)
Rieth, M., Gruber, A., Chen, J.H.: The effect of pressure on lean premixed hydrogenair flames. Combust. Flame **250**, 112514 (2023)
RWTH Aachen University: Cosine research data management. https://docs.coscine.de/en/ (2016). Accessed March 2026
Schlup, J., Blanquart, G.: Reproducing curvature effects due to differential diffusion in tabulated chemistry for premixed flames. **37**(2), 2511–2518 (2019)
Schuh, V., Hasse, C., Nicolai, H.: An extension of the artificially thickened flame approach for premixed hydrogen flames with intrinsic instabilities. Proc. Combust. Inst. **40**(1–4), 105673 (2024)
Shi, S., Schultheis, R., Barlow, R.S., Geyer, D., Dreizler, A., Li, T.: Internal flame structures of thermodiffusive lean premixed H2/air flames with increasing turbulence. Proc. Combust. Inst. **40**(1–4), 105225 (2024)
Sullivan, B., Kaszynski, A.: PyVista: 3D plotting and mesh analysis through a streamlined interface for the visualization toolkit (VTK). J. Educ. Chang. Open Source Softw. **4**(37), 1450 (2019). https://doi.org/10.21105/joss.01450
United Nations: Sustainable development goals. https://www.un.org/sustainabledevelopment/sustainable-development-goals/ (2015). Accessed January 2026
Weller, H., Greenshields, C., Bouffler, B.: OpenFOAM v11. https://openfoam.org/version/11/ (2023). The OpenFOAM Foundation Ltd
Wilkinson, M.D., Dumontier, M., Aalbersberg, I.J., Appleton, G., Axton, M., Baak, A., Blomberg, N., Boiten, J.-W., Silva Santos, L.B., Bourne, P.E., et al.: The FAIR guiding principles for scientific data management and stewardship. Sci. Data **3**(1), 1–9 (2016)

Publisher's Note Springer Nature remains neutral with regard to jurisdictional claims in published maps and institutional affiliations.